Green sonochemical process for preparation of polyethylene glycol–Fe$_3$O$_4$/ZnO magnetic nanocomposite using rambutan peel extract as photocatalyst, for removal of methylene blue in solution

THI MAI HUONG PHAM[1], MINH THANH VU[2], TIEN DUNG CONG[3], NGOC SON NGUYEN[2], TUAN ANH DOAN[2], THI THAO TRUONG[4] and THI HUONG NGUYEN[2,*]

[1] Hanoi University of Industry, Hanoi, Vietnam
[2] Institute of Chemistry and Material, Hanoi 100000, Vietnam
[3] Hanoi University of Mining and Geology, Hanoi, Vietnam
[4] Thai Nguyen University of Science, Thai Nguyen 25000, Vietnam
*Author for correspondence (nguyenhuong0916@gmail.com)

Abstract.   The main objective of this study is the preparation of a polyethylene glycol (PEG)–Fe$_3$O$_4$/ZnO magnetic nanocomposite using a green sonochemical synthesis method with rambutan peel extract as a stabilizing agent for photocatalytic methylene blue (MB) degradation. The synthesized nanocomposites were characterized using field emission scanning electron microscopy, energy dispersive X-ray spectroscopy, Fourier transform infrared spectroscopy (FTIR), X-ray diffraction and UV–visible methods. The field emission scanning electron microscopy results showed the size of nanocomposite was 20–30 nm and had the bandgap energy of 2.58 eV. The effects of the photocatalyst and process time were investigated. The kinetics were investigated, and the regeneration of the photocatalyst was evaluated. Kinetic experiments on MB degradation using the nanocomposite showed good agreement with the Langmuir–Hinshelwood model, and the photocatalyst could remove over 98% of the MB within 90 min.

Keywords.   ZnO/Fe$_3$O$_4$; photocatalytic; magnetic nanoparticles; methylene blue; sonochemical.

1. Introduction

There are many organic dyes, which are widely used in industries such as textiles, paper, cosmetics, food, printing [1–3]. If the waste from these industries is not treated before being discharged into the environment, it will have a big effect on the environment, living organisms and human health, including outcomes such as increased cancer rates, gene mutations and the death of organisms [4–6]. Worldwide, azo dyes are the biggest group of colorants by both production mass and number, making up 70% of all organic dyes [7]. Therefore, in-depth studies have focused on the removal of these persistent organic dyes from water sources. Persistent organic matter treatment methods commonly used are photocatalytic methods [8,9], membrane filtration [10] and coagulation methods [11], biodegradation [12], and adsorption by activated carbon [13,14]. Of these methods, the photocatalytic method, using metal oxide nanocomposites with semiconductors (ZnO, CuO, TiO$_2$, NiO, CoO) under the influence of light to create strong oxidizing radicals to convert persistent organic substances into non-toxic inorganic substances (CO$_2$, H$_2$O), is of research interest [15–17]. ZnO is a group II-VI binary semiconductor with a

wurtzite-type hexagonal structure or pseudo-zinc cubic structure, a bandgap energy of 3.1–3.3 eV and large excitation energy (60 meV) at room temperature. It is used in a variety of technologies, including sensors, optical devices, electrochemical supercapacitors and photocatalysis. Semiconductors have a large band spacing, high excitation bonding energy at room temperature, good physical stability and good chemical stability. The photocatalytic treatment method is environmentally friendly, thorough, and has high efficiency [18,19].

Polyethylene glycol (PEG)–Fe$_3$O$_4$/ZnO nanocomposite materials are aggregated. This results in the combination of the superparameters of the Fe$_3$O$_4$ nanosystem and the ability to rapidly adsorb pollutants and separate them from environmental water.

This is due to characteristic properties such as low superparameter, low toxicity, low electrical conductivity and large specific surface area [20,21]. In addition, instead of using reagents that can cause secondary pollution, rambutan shell extracts are used to synthesize the PEG–Fe$_3$O$_4$/ZnO nanocomposite and combined with ultrasonic wave to increase the dispersion of the system, reduce the size of the catalytic particles and reduce the reaction time.

In the ultrasonic-assisted synthetic (sonochemical synthesis) method, chemical reactions are facilitated by the application of powerful ultrasound radiation (20 kHz–10 MHz). Sonochemistry generates small bubbles that can achieve a high temperature (5000–25000 K), a pressure of more than 1000 atm and a rate of cooling/heating that can exceed 10^{-11} K s^{-1}. They can break chemical bonds or produce chemical and physical effects that can be used for the production or modification of nanostructured materials [22,23]. Ultrasonic-assisted reactions produce smaller sized, purer and more dispersible nanomaterials [24].

In this study, PEG–Fe_3O_4/ZnO magnetic nanocomposites were synthesized on the surface of PEG–Fe_3O_4 in an aqueous solution using ferric chloride hexahydrate ($FeCl_3 \cdot 6H_2O$), ferrous chloride tetrahydrate ($FeCl_2 \cdot 4H_2O$), NH_4OH as the iron precursor and reduction agent, and ZnO nanoparticle powder. The ZnO nanoparticles (20–30 nm) used for preparing the nanocomposite were obtained from 0.1 M zinc nitrate hexahydrate and rambutan peel extract from Vietnam. The photocatalytic activity of the PEG–Fe_3O_4/ZnO magnetic nanocomposite was studied for the removal of methylene blue (MB) under UV light irradiation.

2. Experimental

2.1 *Materials*

The chemicals, ferric chloride hexahydrate ($FeCl_3 \cdot 6H_2O$), ferrous chloride tetrahydrate ($FeCl_2 \cdot 4H_2O$), zinc nitrate hexahydrate ($Zn(NO_3)_2 \cdot 6H_2O$), methylene blue (analytical grade) and PEG polymer (PEG-6000), were purchased from Merck. NH_3 solution and ethanol were provided by Macklin-China, India.

The raw Rambutan (*Nephelium lappaceum L.*) peel was collected from Vietnam Southern, and deionized water was used throughout the study. The Rambutan peel were rinsed with deionized water and dried in the oven at 60°C. The dried Rambutan peel were cut into small pieces and rambutan peel extract was prepared by mixing 3 g of small pieces of Rambutan peel in a Erlenmeyer flask with 100 ml of ethanol/deionized water (1:2, v/v) and boiled at 80°C for 30 min. The extract was cooled and filtered, the rambutan peel extract was kept at 8–10°C for use within a week.
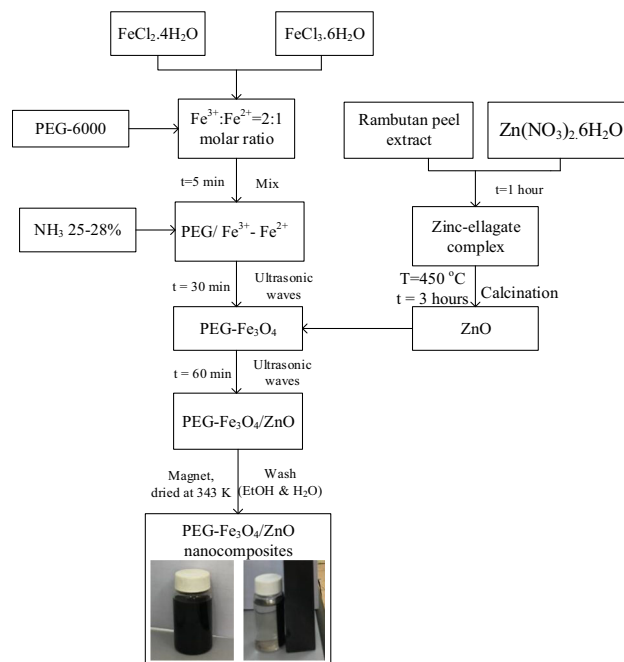
2.2 *Preparation of PEG–Fe_3O_4/ZnO nanocomposite*

Firstly, preparation of the PEG-coated Fe_3O_4 and ZnO nanoparticles: The ZnO nanoparticles were prepared by 0.1 M of zinc nitrate hexahydrate and rambutan peel extract (Vietnam) with constant stirring at room temperature and sonicating for 1 h in an ultrasonic bath (500 W, 20 kHz) [18,25]. The colloid (zinc-ellagate complex) was centrifuged and wased with distlled water. The solid was calcined at 450°C for 3 h to obtain ZnO nanoparticles.

The PEG-coated Fe_3O_4 nanoparticles were prepared by mixing $FeCl_3 \cdot 6H_2O$ and $FeCl_2 \cdot 4H_2O$ at a ratio of 2:1 in deionized water. To this 75 mg l^{-1} PEG was added, using a method published by the authors [20]. The reaction mixture was placed on a sonicator (Sonics & Materials—VCX500; 500 W, 20 kHz), and 25–28% NH_3 solution was added dropwise using a syringe pump at a flow rate of 50 ml h^{-1}. These procedures resulted in the formation of a black precipitate of PEG-coated Fe_3O_4 nanoparticles. ZnO nanoparticles were added to the reaction flask so that the solution was maintained at pH = 8. The system was placed on a sonicator for 1 h at 80°C. A black precipitate was obtained, filtered and washed with distilled water several times until the water became neutral, and then, it was washed twice more with ethanol. The product was dried in an oven at a temperature of 65°C for 24 h. Figure 1 shows the procedure for the preparation of the PEG–Fe_3O_4/ZnO magnetic nanocomposite with ratio of Fe_3O_4:ZnO is 1:4. Corresponding to the element composition from energy dispersive X-ray spectroscopy results showed that PEG–Fe_3O_4/ZnO magnetic nanocomposite contained were 40.46% Zn, 36.53% Cu, 21.00% O and 1.91% C (figure 3d).

2.3 *Characterization*

The crystallinity of Fe_3O_4-NP and ZnO-NP were examined by X-ray diffraction X'Pert Pro-PANalytical instrument. X-ray diffractometer was operated at 1.8 kW (40 mA/45 kV) using CuKα ($\lambda = 1.5406$ Å) radiation. Fourier transform infrared (FTIR) spectra were recorded using the KBr pellet

Figure 1. The procedure for the preparation of PEG–Fe_3O_4/ZnO magnetic nanocomposite.

method, using a Bruker FT-IR spectrometer. Magnetic measurements of the solid samples were performed at room temperature (25°C) using a Magnet B-10 vibrating sample magnetometer (VSM). Field emission scanning electron microscopy analysis was performed using a Hitachi S-4800. A minimal amount of the solid sample was dispersed in ethanol and small drops were placed on an aluminium grid. The grid was dried for 1–2 h in a vacuum at 40°C prior to the field emission scanning electron microscopy studies. UV–Vis diffuse reflectance spectrophotometer (Shimadzu UV-2450) was used to determine the bandgap energy of PEG–Fe_3O_4/ZnO magnetic nanocomposite.

Nitrogen adsorption/desorption data were obtained at 77 K using Tristar 3000-Micromeritics equipment, USA. Samples were degassed at 75°C and 10^{-6} Torr for a minimum of 12 h prior to analysis. The specific surface area was calculated from the linear part of the BET plot according to IUPAC recommendation, and the pore size was determined using the BJH (Barrett–Joyner–Halenda) model.

2.4 Photocatalytic activity of the PEG–Fe₃O₄/ZnO magnetic nanocomposite

To determine the photocatalytic activity of the PEG–Fe_3O_4/ZnO magnetic nanocomposite, the removal of MB under UV light was studied.

The photocatalytic activity of the prepared photocatalysts was evaluated by monitoring the decomposition rate of aqueous MB solution. The photocatalytic activity experiments were carried out to investigate the influence of parameters that have a major effect on the decomposition rate of MB: pH, contact time, initial concentration of MB and amount of catalyst powder. In these experiments, a fixed quantity of Fe_3O_4/ZnO nanocomposite was mixed with a specific volume of MB and constantly shaken at room temperature, until equilibrium was reached. After the photocatalysis, the solutions were filtered through Whatman no. 42 filter paper. The filtrate was collected in polyethylene tubes and diluted before analysis. During the study, the catalyst powder used was varied from 0.5 to 2.0 g l^{-1}, the pH from 2.0 to 10.0, the initial MB concentration from 50 to 200 mg l^{-1}, and the contact time from 0 to 120 min. Hydrogen peroxide was added as a radical agent. The pH of the solution was adjusted to the required value using either 0.1 N HCl or 0.1 N NaOH solution.

For the adsorption isotherms, a series of 100 ml glass flasks were filled with 50 ml of MB solution of varying concentrations and maintained at the desired temperature and pH, to which 1.0 g l^{-1} of PEG-Fe_3O_4/ZnO nanocomposite was added. An optimum uptake time of 60 min for MB was calculated by taking the difference in the initial and final concentrations. In each experiment, the removal of MB was carried out in the dark. All the experiments were repeated three times and average values were reported.

The photocatalytic activity of the synthesized catalyst was estimated by measuring the residual concentration of MB dye in the solution. Spectrophotometric analysis of the dye was used to determine its decolorization efficiency. The absorbance of the MB dye was measured using a UV–visible spectrophotometer. The maximum wavelength of absorbance for the MB dye is $\lambda_{max} = 663$ nm.

2.5 Kinetic studies of MB degradation in PEG–Fe₃O₄/ZnO

The photocatalytic oxidation kinetics of MB compounds have often been modelled using the Langmuir–Hinshelwood equation. The fitting of experimental data to Langmuir–Hinshelwood kinetic model has been demonstrated for the photocatalytic oxidation of organic dyes [26,27]. This model is expressed by the following equation:

$$\frac{1}{k_{app}} = \frac{1}{k_c K_{LH}} + \frac{[MB]_0}{k_c}, \tag{1}$$

where $[MB]_0$ is the initial concentration of MB compound (mg l^{-1}), K_{LH} is the Langmuir–Hinshelwood adsorption equilibrium constant (l mg^{-1}), k_c is the rate constant of the surface reaction (mg l^{-1} min^{-1}), and k_{app} is the apparent constant of degradation.

The photocatalysis (the degradation of aqueous MB solution containing PEG–Fe_3O_4/ZnO by UV irradiation, involving the adsorption of the substrate on the photocatalyst surface) follows pseudo-first-order kinetics. This model is expressed by the equation:

$$r = -\frac{dC}{dt} = k_{app}C, \tag{2}$$

where r is the degradation rate (mg l^{-1} min^{-1}), k_{app} is the apparent constant of degradation (l min^{-1}), and C the concentration of the organic substrate at time t (mg l^{-1}).

The integration of this equation (with limitation $C = C_0$ for $t = 0$) leads to the following equation:

$$\ln\frac{C_0}{C} = k_{app}t. \tag{3}$$

The mathematical models developed by Langmuir have been applied to the irradiation of MB with PEG–Fe_3O_4/ZnO nanocomposites. The Langmuir isotherm model can be expressed linearly as in equation (4) [28]:

$$\frac{C_t}{Q} = \frac{1}{q_{max}K_L} + \frac{C_t}{q_{max}}. \tag{4}$$

where C_t is the concentration of MB (mg l^{-1}) at equilibrium, q_{max} is the monolayer capacity of the adsorbent (mg g^{-1}) and K_L the Langmuir sorption constant (l mg^{-1}). The plot of C_t/Q vs. C_t was a straight line (figure 6) and the values of q_{max} and K_L can be calculated from the slope and intercept of the plots.

3.   Results and discussion

3.1   *Structural and morphological studies*

During the preparation of PEG-coated Fe_3O_4 nanoparticles, ZnO nanoparticles and Fe_3O_4/ZnO magnetic nanoparticles, the colour of the reaction mixtures changed several times due to the influence of the phase of the compound formed.

First, ammonia solution, which was added to the reaction solution, produces OH^- anions, which react with Fe^{2+} and Fe^{3+} cations to form Fe_3O_4 nanoparticles. The addition of PEG to the reaction mixture resulted in the Fe_3O_4 being coated with PEG. Due to the interaction between the OH groups of the PEG compound and the OH groups on the surface of Fe_3O_4 nanoparticles, H atoms were released, and the C–H chain interacted with the Fe_3O_4 surface [29]. The preparation of ZnO nanoparticles, and the formation of ester oxygen atoms and phenolic hydroxy groups of polyphenols result in a p-track conjugation effect, in which hydroxyl groups bind with the metal. A zinc-ellagate complex formed due to the chelating effect. The direct decomposition of the zinc-ellagate complex at 450°C led to ZnO nanoparticles [25]. Then, the ZnO nanoparticles were functionalized to form the PEG–Fe_3O_4, as shown in figure 1. The products were characterized using powder X-ray diffraction (XRD), FTIR and VSM methods. Figure 2a shows the XRD patterns and FTIR spectra of the PEG–Fe_3O_4/ZnO samples. The positions and relative intensities of the diffraction peaks in all the XRD patterns were fully matched. In addition, all the diffraction peaks were in good agreement with the standard card of Fe_3O_4 (ICSD code: 028664) and ZnO (ICSD code: 065122). The characteristic peaks of Fe_3O_4, namely the peaks at 2θ of 30.0°, 35.4°, 57.2° and 62.6°, indicated that the Fe_3O_4 nanoparticles had a cubic spinel structure [30]. The peaks for ZnO, at 2θ of 31.76°, 34.28°, 36.12°, 47.30°, 56.37° and 68.77°, indicated that the ZnO nanoparticles had

a hexagonal structure [25,31]. In order to estimate the crystallite sizes, we have used both the Scherrer equation and the Williamson-Hall plot. The results show that the crystal sizes of Fe_3O_4 in PEG–Fe_3O_4 and PEG–Fe_3O_4/ZnO nanocomposite materials are 20.94 and 16.77 nm, respectively. The size of ZnO crystals is 21.09 nm.

Figure 2b shows the FTIR spectrum of the prepared PEG–Fe_3O_4/ZnO nanocomposites. The surface of the ZnO nanoparticle powder shows the presence of metabolites in the rambutan peel extract, such as phenolic acids, proanthocyanidins, tannins, flavonoids, fatty acids, pectin, carotenoids, sugars and fruit acids such as ascorbic acid, malic acid, and citric metabolites, which possess antioxidant activity [25]. The biocapping phenomenon could be due to the presence of metabolites such as phenolic and carboxylic acids that adhered to the surface of the ZnO nanoparticles. The spectrum obtained for the PEG–Fe_3O_4/ZnO nanocomposite clearly shows Zn–O absorption bands at 456 cm^{-1} [21]. Bands at 1109 and 1058 cm^{-1}, corresponding to the C–O stretching mode of esters, were not present. However, the significant absorption peaks at 3429, 628 cm^{-1} could be assigned to O–H stretching and H–O–H bending vibration due to the adsorption of moisture, and Zn–O stretching vibration, respectively. In the FTIR spectrum of PEG–Fe_3O_4/ZnO, there is also a sharp absorption in the finger-print range at 564 cm^{-1}, indicating the presence of an Fe–O bond in the pure Fe_3O_4 and Fe_3O_4–PEG samples [20,32].

Figure 3a shows that the PEG–Fe_3O_4 surface material has particle sizes in the range of 10–30 nm. Cubic particles are less uniform and have a smooth surface. The images of the nanocomposite material at different magnifications show a distribution of Fe_3O_4 and ZnO nanoparticles with dimensions less than 30 nm. The synthetic nanocomposite material therefore has a larger surface area than the base material, which is shown using measurements of the specific surface area using the BET technique. The porosity
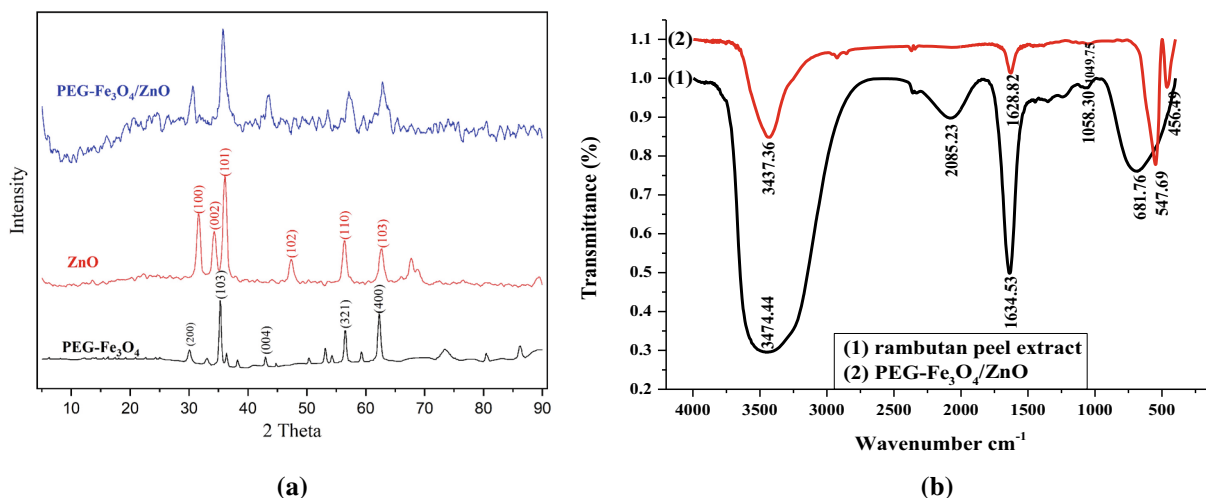
Figure 2.   (**a**) XRD patterns of the ZnO, PEG–Fe_3O_4 and PEG–Fe_3O_4/ZnO samples. (**b**) FTIR spectra of the rambutan peel extract and PEG–Fe_3O_4/ZnO.
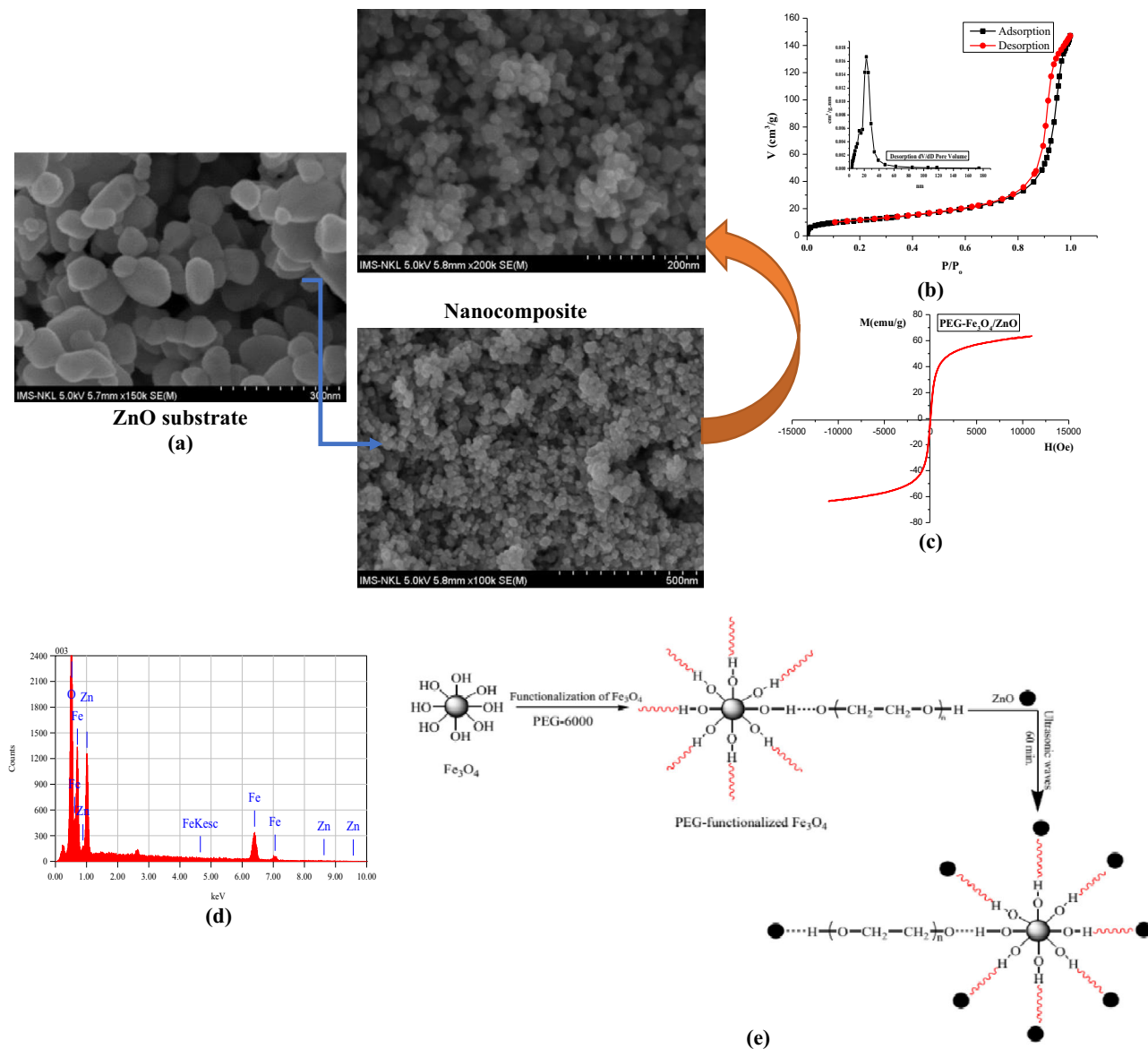
Figure 3. (**a**) Field emission scanning electron microscopy images of the PEG–Fe$_3$O$_4$/ZnO. (**b**) Nitrogen adsorption–desorption isotherms for the PEG–Fe$_3$O$_4$/ZnO. (**c**) M–H curves for the PEG–Fe$_3$O$_4$/ZnO. (**d**) Energy dispersive X-ray spectroscopy image of PEG–Fe$_3$O$_4$/ZnO. (**e**) Schematic illustration of the preparation process for the PEG–Fe$_3$O$_4$/ZnO magnetic nanocomposites.

characteristics of the PEG–Fe$_3$O$_4$/ZnO nanocomposite were studied using BET nitrogen physisorption at –196.15°C.

Figure 3b shows the adsorption–desorption isotherm for the PEG–Fe$_3$O$_4$/ZnO nanocomposite. The adsorption–desorption isotherm is of type IV, as typified by the H3 hysteresis loop, rod-shaped and letter-shaped according to IUPAC classification [33]. This allows us to predict that the synthetic nanocomposite materials contain both macropores and mesopores, with the mesopores being more numerous. The isotherm has two inflection points due to nitrogen uptake. The first is slow at a low relative pressure (<0.1), and the second is sharp at a relative pressure of about 0.95, with a hysteresis loop at a relative pressure above 0.7. The higher nitrogen uptake at low relative pressure is indicative of monolayer adsorption, whereas the sharp uptake at a higher relative pressure shows multilayer adsorption. The pore size distribution is obtained from BJH analysis. The BJH pore size distribution curve shows narrow and intense peaks. The hole size distribution curve shows that holes appear in the range 3 to 170 nm. The specific surface area of the ZnO surface material (synthesis by a chemical method) is 2.10 m^2 g^{-1}, which is much smaller than that of the nanocomposite material, which reaches 40.52 m^2 g^{-1}. The micropore area of the nanocomposite $S_{micro} = S_{BET} - S_{external} = 0.77$ m^2 g^{-1}, the pore diameter averages 22.3 nm, and the total pore volume is 0.24 cm^3 g^{-1}.

The magnetic properties of the materials were assessed using vibrating sample magnetometry (figure 3c). The

saturation magnetization of the PEG–Fe$_3$O$_4$/ZnO nanocomposite was 65.2 emu g^{-1}. This indicates that the sample was superparamagnetic, and the iron oxide particles were nanosized and distributed on the soluble surface. Therefore, it is convenient to separate this material from the aqueous solution after adsorption with the help of an external magnetic field [34].

The value of the energy gap (E_g) of the bulk ZnO is 3.31 eV, but or a thin film, the E_g value depends on the manufacturing technique [35,36]. The optical energy gap can be estimated by calculating the absorption coefficient (α), which depends on the film thickness (the length of the absorption media) and the absorbance, as shown in the following equation:

$$\alpha = 2.303 \left(\frac{A}{d} \right), \tag{5}$$

where A is the absorbance and d the thickness. The energy gap can be estimated by assuming direct and indirect allowed transitions between the valence and conduction bands using the Tauc equation [35,36]:

$$\alpha h\vartheta = B \left(h\vartheta - E_g \right)^r, \tag{6}$$

where B is a constant, α is the absorption coefficient, $h\vartheta$ is the incident photon energy, and r a constant. For direct transition $r = 1/2$, and for indirect transition $r = 2$.

Figure 4 shows $(\alpha h\vartheta)^2$ plotted against $h\vartheta$. The bandgap of the nanocomposite, E_g, was determined by extrapolating the linear section of the plot to the $h\vartheta$ axis at $(\alpha h\vartheta)^2 = 0$. The Fe$_3O_4$/ZnO nanocomposite has a direct allowed energy bandgap of 2.58 eV. This bandgap lies between those of ZnO (3.32 eV) and Fe$_3$O$_4$ (0 eV). Therefore, by tuning the volume fractions of the constituent oxides, the bandgap can be engineered to make the nanocomposite suitable for several applications such as in photovoltaics, solid oxide fuel cells, photocatalysis and thermoelectric.
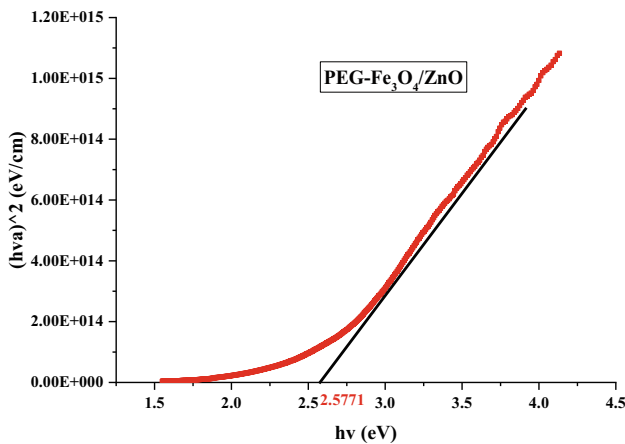
## 3.2 *Photocatalytic activity of the PEG–Fe$_3$O$_4$/ZnO nanocomposites*

The photocatalytic activity of the nanocomposites was measured with 1.0 g l^{-1} of PEG–Fe$_3$O$_4$/ZnO and a pH of 4 under the following conditions: (1) irradiation of MB with UV light in the absence of the PEG–Fe$_3$O$_4$/ZnO nanocomposite; (2) MB in the dark in the presence of the PEG–Fe$_3$O$_4$/ZnO nanocomposite; and (3) irradiation of MB with UV light in the presence of the PEG–Fe$_3$O$_4$/ZnO nanocomposite. The results of the studies are shown in figures 5 and 6. Figure 6 shows the establishment of Langmuir adsorption constants for the adsorption of MB on the PEG–Fe$_3$O$_4$/ZnO in the dark.

The results in figure 5 show that there was no significant degradation under UV light in the absence of the PEG–Fe$_3$O$_4$/ZnO nanocomposite. In the dark, when in the presence of the nanocomposite without irradiation, the catalyst caused 28.8% degradation of MB. This loss was observed due to the adsorption of MB on the surface of the PEG–Fe$_3$O$_4$/ZnO nanocomposite. The irradiation of MB under UV light in the presence of the PEG–Fe$_3$O$_4$/ZnO nanocomposite resulted in >98% degradation in 90 min. These results show that the nanocomposite material is both adsorbent and catalytic. The adsorption process supports the MB degradation catalytic process, reducing the decomposition time and increasing the efficiency of the catalytic process. This contrasts with ZnO nanoparticle materials, which play a major role only in the catalytic process—the adsorption process hardly occurs at all [21,37].

The results in figure 6 show that the Langmuir adsorption constant and the maximum adsorbable quantity of MB were calculated as $K_L = 0.0451$ l mg^{-1} and $Q_{max} = 21.05$ mg g^{-1}. These results show that the maximum adsorption capacity of the synthesized nanocomposite is greater than that of some previously published ZnO nanoparticles [38].

Figure 4.   Bandgap of the PEG–Fe$_3$O$_4$/ZnO nanocomposite.
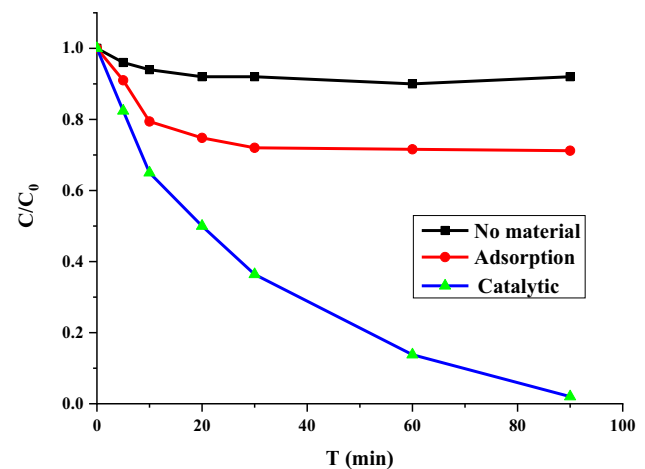
Figure 5.   Removal efficiency of methylene blue for [PEG–Fe$_3$O$_4$/ZnO] = 1.0 g l^{-1}, [methylene blue] = 50 mg l^{-1}, pH = 4, and t = 90 min.
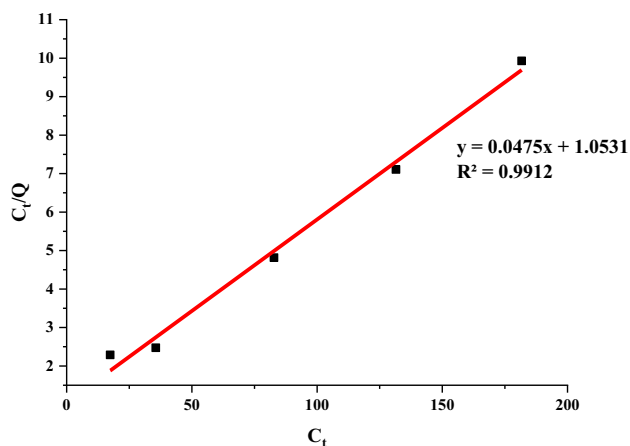
Figure 6. Establishment of Langmuir adsorption constants for the adsorption of methylene blue on PEG–Fe₃O₄/ZnO.

3.2a *Effect of initial pH:*   pH has the most important role in the photocatalytic study. It controls the reactions during the degradation of MB, and the generation of hydroxyl radicals also depends on the pH of the solution [39]. The effect of pH on the photocatalytic degradation of MB in the range of pH 2 to 10 in the presence of the PEG–Fe₃O₄/ZnO nanocomposite is shown in figure 7.

The degradation rate of PEG–Fe₃O₄/ZnO is at a maximum at acidic pH (pH = 2 to 4) and decreases with increasing pH. The pH of the solution affects the surface charge properties of the catalyst and the adsorption behaviour. When the pH is less than 4, the dissolution of Fe_3O_4 nanoparticles occurs [40]. Therefore, pH = 4 was chosen for the later investigations.

3.2b *Effect of the amount of PEG–Fe₃O₄/ZnO nanocomposite:* The degradation percentages of MB with different catalyst doses between 0.5 and 2.0 g l^{-1}
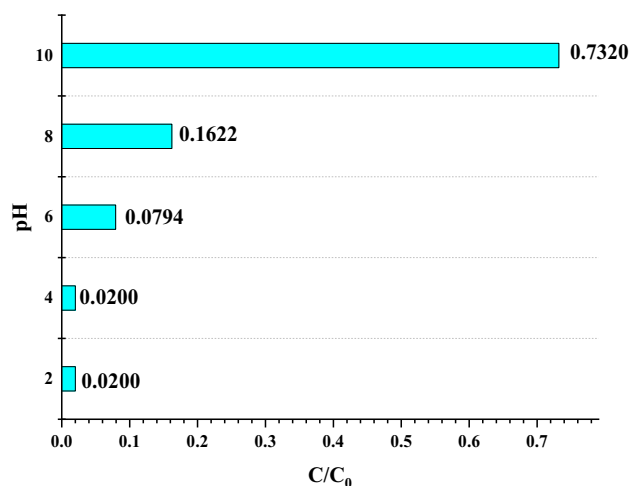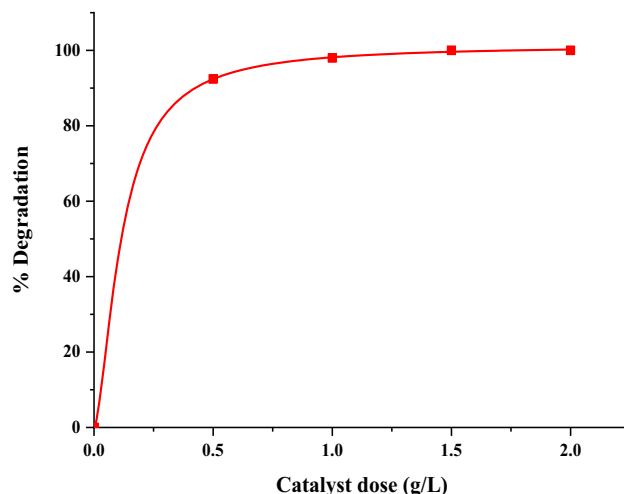
were measured. The results in figure 8 show that the rate of degradation increased as the PEG–Fe₃O₄/ZnO catalyst concentration increased. When the catalyst concentration was increased above 1 g l^{-1}, the degradation of MB was approximately 100%. This is the major factor reducing light absorption by the photocatalyst. The agglomeration prevents photons from reaching the inner layers of the catalyst. Fewer catalyst particles get excited, and ultimately fewer electrons/holes and hydroxyl radicals are produced. Therefore, the degradation rate tends to decrease as the catalyst dose increases [41,42].

3.2c *Effect of initial concentration of methylene blue:* The effect of initial MB concentration on the degradation efficiency was studied at the optimized pH of 4 by varying the initial dye concentrations (from 50 to 200 mg l^{-1}). The results in figure 9 show a maximum degradation at the initial dye concentration of 50 to 200 mg l^{-1}, when the maximum degradation of MB dye was approximately 96%. The degradation efficiency of the dye decreased when the initial concentration of dye was increased. Therefore, the hydroxyl radicals produced are insufficient for the degradation of the dye at high concentration. Therefore, the photodegradation efficiency is reduced as the concentration of the dye increases [43].

3.2d *Kinetic studies of MB in the PEG–Fe₃O₄/ZnO nanocomposite UV process:*   Linear plots of Ln(C_0/C) as a function of contact time are shown in figure 10. The results show that the photocatalytic degradation of MB was pseudo-first order. Ln(C_0/C) is directly proportional to the contact time. This indicates that the photocatalytic degradation of MB solution is directly proportional to the concentration of the MB dye solution and directly proportional to the contact time. Because of this, we can conclude that the photocatalytic degradation is a pseudo-

Figure 7. Effect of pH on the photocatalytic degradation of methylene blue at [PEG–Fe₃O₄/ZnO] = 1.0 g l^{-1}, [methylene blue] = 50 mg l^{-1} and *t* = 90 min.

Figure 8. Effect of catalyst dose on the photocatalytic degradation of methylene blue at pH = 4.0, [methylene blue] = 50 mg l^{-1} and t = 90 min.
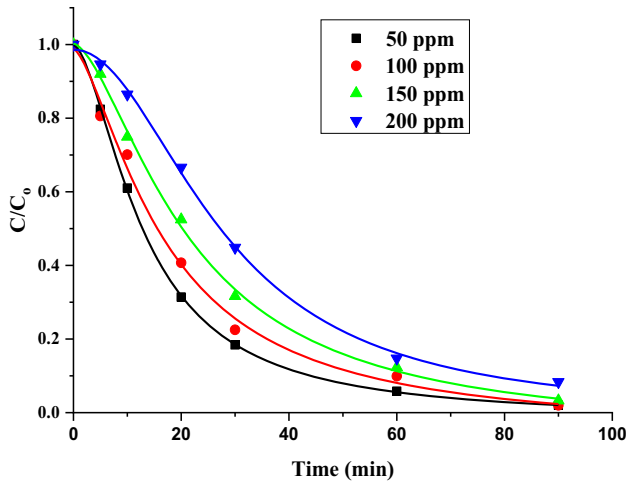
Figure 9. Effect of initial methylene blue concentration on the photocatalytic degradation at pH = 4.0, [PEG–Fe$_3$O$_4$/ZnO] = 1.0 g l^{-1}, [methylene blue] = 50–200 mg l^{-1} and t = 90 min.
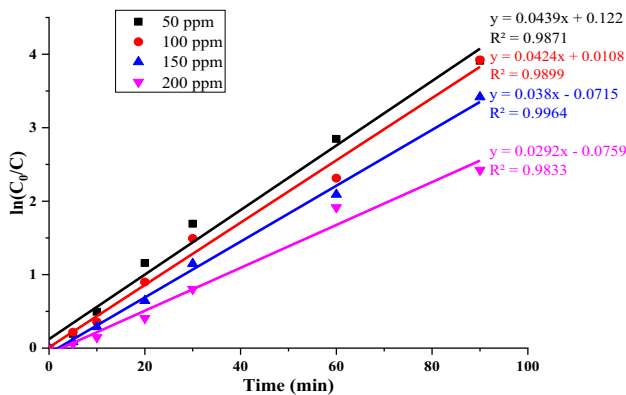
Figure 10. Kinetic fits for the photocatalytic degradation of methylene blue at pH = 4.0, [PEG–Fe$_3$O$_4$/ZnO] = 1.0 g l^{-1}, [methylene blue] = 50–200 mg l^{-1} and t = 90 min.

first-order reaction. We can compare the k values and linear regression coefficients R^2 for MB solution with different initial concentrations. These data are summarized in table 1. The k values were obtained by linear fitting from the graph. Figure 11 shows the variation of reciprocal of the rate constant with the initial concentration of MB.
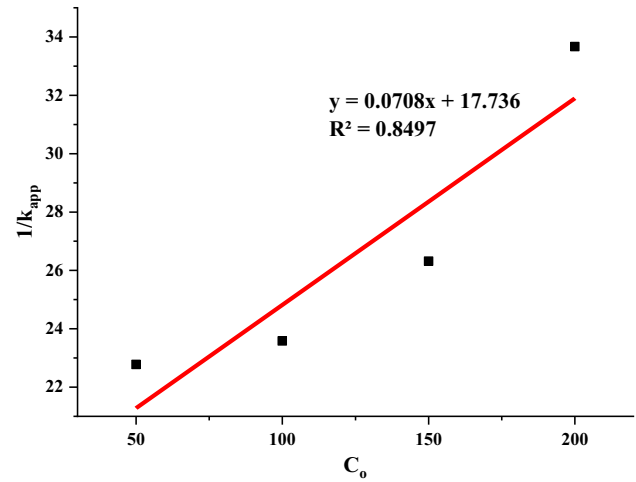
Figure 11. Variation of the reciprocal of the rate constant with the initial concentration of methylene blue.

According to equation (1), a plot of $1/k_{app}$ *vs.* the initial concentration of MB (C_0) should be linear. Figure 11 shows this to be the case, confirming the Langmuir–Hinshelwood relationship for initial rates of degradation (k_c).
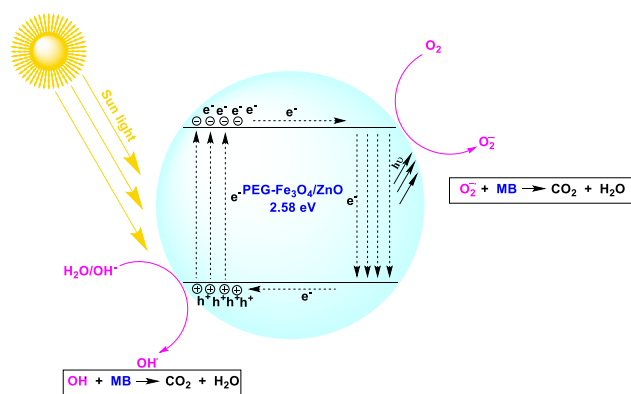
The values of related parameters and constants k for the photocatalytic degradation reaction are shown in table 1. As the results show, the obtained data fit a pseudo-first-order reaction (R^2 = 0.9833–0.9964). The adsorption constant in the kinetic model determined in our case was found to be close to that obtained in the dark, K_L = 11.275 K_{LH}, and the photocatalytic degradation of 200 mg l^{-1} of MB at pH = 4.0 and 1 g l^{-1} of PEG–Fe$_3$O$_4$/ZnO follows satisfactorily the Langmuir–Hinshelwood model. Similar results have been reported in other studies. For example, it was reported that K_{LH} measured under irradiation could be substantially different from K_L measured in the dark [44].

The decomposition of MB in solution has been explained by the use of free radicals on MB agents [45]. Firstly, the electron/pore pair is produced with the adsorption of solar light by PEG–Fe$_3$O$_4$/ZnO nanocomposite and increasing the band energy (>2.57 eV). The h$^+_{VB}$ generates $^•$OH by transferring and depleting OH$^-$ ions or by H$_2$O. Then, the surface of O$_2$ by adsorption and condensation of bond electrons produces anionic superoxide radicals (O$_2^-$), which can react with protons (H$^+$) to form OOH radicals. The

Table 1. Kinetic parameters for the photocatalytic degradation and photocatalytic oxidation of methylene blue, and values of the Langmuir–Hinshelwood constant and the rate constant of the surface reaction.

C_0 (ppm)	R^2	k_{app} (min^{-1})	k_c (mg l^{-1} min^{-1})	K_{LH} (l mg^{-1})
50	0.9771	0.0439	14.123	0.004
100	0.9899	0.0424		
150	0.9964	0.0380		
200	0.9833	0.0292		

Figure 12. Photocatalyic reaction mechanism of PEG–Fe$_3$O$_4$/ZnO nanocomposite.

photocatalytic reaction mechanism of PEG–Fe$_3$O$_4$/ZnO nanocomposite is shown in figure 12.

4. Conclusion

PEG–Fe$_3$O$_4$/ZnO magnetic nanocomposite photocatalysts were synthesized using a green sonochemical synthesis method with rambutan peel extract. XRD patterns revealed that the ZnO nanoparticles had a hexagonal structure, and the IR spectrum clearly showed Zn–O absorption bands at 456 cm^{-1}, assigned to Fe$_3$O$_4$/ZnO nanocomposites. The FTIR spectrum of PEG–Fe$_3$O$_4$/ZnO showed sharp adsorption at 564 cm^{-1} in the fingerprint range, indicating the presence of an Fe–O bond in the Fe$_3$O$_4$–PEG samples. The average crystallite sizes of the ZnO and Fe$_3$O$_4$ samples were calculated to be 22.09 and 11.96 nm, respectively. The results of this study show that the doping of ZnO nanoparticles with PEG–Fe$_3$O$_4$ improves the photocatalytic properties of ZnO, and the Fe$_3$O$_4$/ZnO nanocomposite has a direct allowed energy bandgap of 2.58 eV. Measurements of the degradation efficiency of the photocatalyst showed that the photocatalytic degradation of MB follows pseudo-first-order kinetics with good correlation and linear regression coefficient. This study found that the maximum degradation of the MB dye was approximately 96%, with pH = 4.0, a PEG–Fe$_3$O$_4$/ZnO concentration of 1.0 g l^{-1}, a MB concentration of 200 mg l^{-1}, and a time of 90 min. In the dark, the Langmuir adsorption constant and the maximum adsorbable MB quantity were calculated as $K_{\mathrm{L}} = 0.0451$ l mg^{-1} (and $K_{\mathrm{L}} = 11.275\ K_{\mathrm{LH}}$) and $Q_{\max} = 21.05$ mg g^{-1}. This study concludes that for the Fe$_3$O$_4$/ZnO magnetic nanocomposite, the adsorption process supports catalytic MB degradation, reducing the decomposition time, increasing the efficiency of the catalytic process, and increasing the sample recovery due to the magnetic properties of the material.

References

[1] Travis Anthony S, Hornix Willem J, Bud R and Hornix Willem J 1992 *Br. J. Hist. Sci.* **25** 65

[2] Rajeshwar K and Ibanez Jorge I G (eds) 1997 *Environmental electrochemistry: fundamentals and applications in pollution sensors and abatement* (California: Academic Press)

[3] Bafana A, Devi S S and Chakrabarti T 2011 *Environ Rev.* **19** 350

[4] Verma Y 2008 *Toxicol. Ind. Health* **24** 491

[5] Lellis B, Fávaro-Polonio C Z, Pamphile J A and Polonio J C 2019 *Biotechnol Res. Innov.* **3** 275

[6] Milani D, Bartlett A J, de Solla S R, Parrott J L, Intini K D, Legault D et al 2018 *Environ. Sci. Pollut. R* **25** 6937

[7] Carliell C M, Barclay S J, Shaw C, Wheatley A D and Buckley C A 1998 *Environ. Technol.* **19** 1133

[8] Rajeshwar K, Osugi M E, Chanmanee W, Chenthamarakshan C R, Zanoni M V B, Ka- Jitvichyanukul P et al 2008 *J. Photochem. Photobiol. C* **9** 171

[9] Isa K and Shrivastava V S 2019 *J. Water Environ. Nanotechnol.* **4** 251

[10] Chidambaram T and Michael N 2015 *Crit. Rev. Env. Sci. Tec.* **45** 1007

[11] Aydıner C, Kaya Y, BerilGönder Z and İlda V 2010 *J. Chem. Technol. Biot.* **85** 1229

[12] Radia J and Romana S 2019 *Eur. J. Microbiol. Immunol.* **9** 114

[13] Foo K and Hameed B 2012 *Desalin. Water Treat.* **19** 255

[14] Syafalni S, Sing S R B and Zawawi M H 2014 *World Appl. Sci. J.* **32** 818

[15] Lalitha G, Hemamalini R, Saravanan R, Ravichandran K, Gracia F, Agarwal S et al 2017 *J. Photochem. Photobiol. B* **173** 43

[16] Chen R X, Zhu S L, Mao J, Cui Z D, Yang X J, Liang Y Q et al 2015 *Int. J. Photoenergy* **2015** ID 183468

[17] Fang H, Guo Y, Wu T and Liu Y 2018 *New J. Chem.* **42** ID 12779

[18] Aminuzzaman M, Ying P L, Goh W-S and Watanabe A 2018 *B Mater. Sci.* **41** 50

[19] Agarwal H, Kumar S V and Rajeshkumar S 2017 *Resour. Efficient Technol.* **3** 406

[20] Huong N T, Son N N, Phuong V H, Dung C T, Huong P T M and Son L T 2020 *Adsorpt. Sci. Technol.* **38** 483

[21] Farrokhi M, Hosseini S C, Yang J K and Shirzad-Siboni M 2014 *Water Air Soil Poll.* **225** 2113

[22] Qiao S Z, Liu J, Lu G Q, Ruren X and Yan X 2005 *Modern inorganic synthetic chemistry* (The Netherlands: Elsevier) p 613

[23] Aharon G 2004 *Ultrason. Sonochem.* **11** 47

[24] Jiang H, Yan Z, Zhao Y, Hu X and Lian H 2021 *Talanta* **94** 251

[25] Yuvakkumar R, Suresh J, Nathanael A J, Sundrarajan M and Hong S I 2014 *Mater. Sci. Eng. C* **41** 17

[26] Vasanthkumar K, Porkodi K and Selva-Ganapathi A 2007 *Dyes Pigm.* **75** 246

[27] Rodriguez-Acosta J W, Mueses M and Machuca-Martínez F 2014 *Int. J. Photoenergy* Article ID 817538

[28] Ossman M, Mansour M and Fattah M 2014 *Bulg. Chem. Commun.* **46** 629

[29] Bagheri S and Julkapli N M 2016 *J. Magn. Magn. Mater.* **416** 117

[30] Daou T J, Pourroy G, Bégin-Colin S, Grenèche J M, Ulhaq-Bouillet C, Legaré P *et al* 2006 *Chem. Mater.* **18** 4399

[31] Ochieng P E, Iwuoha E, Michira I, Masikini M, Ondiek J, Githira P *et al* 2015 *Int. J. Biochem. Phys.* **23** 53

[32] Li Z, Wei L, Gao M Y and Lei H 2005 *J. Adv. Mater.* **17** 1001

[33] Matthias T, Katsumi K, Neimark Alexander V, Olivier James P, Francisco R-R, Jean R *et al* 2015 *Pure Appl. Chem.* **87** 1051

[34] Lv X, Xue X and Jiang G 2014 *J. Colloid Interface Sci.* **417** 51

[35] Alhamed M and Abdullah W 2010 *J. Electron Dev.* **7** 246

[36] Ghodsi F E and Absalan H 2010 *Acta Phys. Pol. A* **118** 659

[37] Benhebal H, Chaib M, Salomon T, Geens J, Leonard A, Lambert S D *et al* 2013 *Alex. Eng. J.* **52** 517

[38] Xueqing Y, Duan Wenyan L, Yan Z F and Ruijun Z 2011 *Bull. Mater. Sci.* **34** 1569

[39] Kannappan V and Santhi J 2004 *Indian J. Chem.* **43A** 1431

[40] Mahmood I, Chen G, Yueping G, Ahmad I and Huizhou L 2010 *J. Hazard. Mater.* **181** 1039

[41] Adiq M M and Nesaraj A S 2014 *Iran. J. Catal.* **4** 219

[42] Ajoudanian N and Nezamzadeh-Ejhieh A 2015 *Mat. Sci. Semicon. Proc.* **36** 162

[43] Marathe Yogesh V, Ramanna M M V and Shrivastava V S 2013 *Water Treat.* **51** 5813

[44] Sauer T, Neto G C, José H J and Moreira R F P M 2002 *J. Photochem. Photobiol. A* **149** 147

[45] Rania E, Hannaa S, Zakaria K, Ahmed H M, Sadeek A S, Sharaa S I *et al* 2021 *Environ. Technol. Innov.* **23** 101710